

# Computer simulations of the two-dimensional melting transition using hard disks

A. Jaster

Universität - GH Siegen, D-57068 Siegen, Germany

February 7, 2008

## Abstract

We present detailed Monte Carlo results for the two-dimensional melting transition of various systems up to  $N = 65536$  hard disks. The simulations are performed in the  $NVT$  ensemble, using a new updating scheme. In the isotropic phase the bond orientational correlation length  $\xi_6$  and the susceptibility  $\chi_6$  are measured and compared with the predictions of the Kosterlitz-Thouless-Halperin-Nelson-Young (KTHNY) theory. From the scaling relation of  $\xi_6$  and  $\chi_6$  we calculate the critical exponent  $\eta_6$ . In the phase transition region we use finite-size scaling methods to locate the disclination binding transition point and compare the results with the values obtained from the behaviour in the isotropic phase. Additionally, we measure the topological defect density, the pressure and the distribution of the second moment of the local bond orientational order parameter. All results are in good agreement with the KTHNY theory, while a first-order phase transition with small correlation length and a one-stage continuous transition can be ruled out.

PACS: 64.70.Dv, 64.60.Fr

## 1 Introduction

The nature of the two-dimensional melting transition is a long unsolved problem [1, 2]. Melting in two dimensions differs from the three-dimensional case because the two-dimensional solid possesses only quasi-long-range positional order, while the three-dimensional solid is truly long-range positionally ordered. This means that the correlation function in two dimensions decays algebraically to zero for large distances, while it decays to a non-zero value in three dimensions. This absence of conventional long-range order at non-zero temperatures in two dimensions was pointed out by Mermin and Wagner [3]. Therefore, the mean-square displacement of the particles from their ideal lattice position will diverge logarithmically with the size of the system and no Bragg peaks in a strict manner can occur in the thermodynamic limit. Nevertheless, the other order parameter, which describes the bond orientational order, is truly long-ranged ordered, i.e. the orientation of the bonds between neighbored particles is correlated over arbitrary distances.

There are several theoretical approaches for the description of melting in two dimensions. Halperin and Nelson as well as Young have developed a theory based on the ideas of Kosterlitz and Thouless [4]. The KTHNY theory deals with unbinding scenarios of topological defects, where the two order parameters are related to two different topological defects: the disclinations and the dislocations. The dislocation unbinding at a temperature  $T_m$  is responsible for the melting transition, while the disclination unbinding at  $T_i$  destroys the bond orientation. The first continuous transition transforms the solid into a novel hexatic phase, which is short-ranged positional and quasi-long-ranged orientational ordered. The second continuous transition transforms this hexatic phase in an isotropic one, i.e. a phase with short-ranged positional and orientational order. An alternative scenario has been proposed by Chui [5]. He presented a theory via spontaneous generation of grain boundaries, i.e. collective excitations of dislocations. He found that grain boundaries may be generated before the dislocations unbind if the core energy of dislocations is sufficiently small, and predicted a first-order transition. This is characterized by a coexistence region of the solid and isotropic phase, while no hexatic phase exists. Another proposal was given by Glaser and Clark [2]. They considered a detailed theory where the transition is handled as a condensation of localized, thermally generated geometrical defects and found also a first-order transition. Calculations based on the density-functional approach were done by Ryzhov and Tareyeva [6]. They derived that the hexatic phase cannot exist in the hard disk system.

Numerical investigations of two-dimensional melting can be done in several ways. On the one hand one can simulate the particle system or the defect system [7], on the other hand one can study lattice models which describe defects and their elastic interaction [8] or grain boundaries [9].

The hard disk system is one of the simplest particle models to study the melting transition in two dimensions with computer simulation techniques. Even for this simple case no consensus about the existence of an hexatic phase has been established. The melting transition of the hard disk system was first seen in a computer simulation by Alder and Wainwright [10]. They used a system of  $N = 870$  disks, constant volume  $V$  and molecular dynamics methods ( $NVE$  ensemble) and found that this system undergoes a first-order phase transition from the solid to the isotropic phase. However, the results of such small systems are affected by large finite-size effects. Simulations performed in the last years used Monte Carlo (MC) techniques either with constant volume ( $NVT$  ensemble) [11, 12, 13, 14] or constant pressure ( $NpT$  ensemble) [15, 16]. Zollweg, Chester and Leung [11] made detailed investigations of large systems up to 16384 particles, but draw no conclusions about the order of the phase transition. The analysis of Zollweg and Chester [12] for the pressure gave an upper limit for a first-order phase transition, but is compatible with all other scenarios. Lee and Strandburg [15] used isobaric MC simulations and found a double-peaked structure in the volume distribution. Lee-Kosterlitz scaling led them to conclude that the phase transition is of first order. However, the data are not in the scaling region, since their largest system contained only 400 particles. MC investigations of the bond orientational order parameter via finite-size scaling with the block analysis technique of 16384 particle systems were done by Weber, Marx and Binder [13]. They also favoured a first-order phase transition. In contrast to this, Fernández, Alonso and Stankiewicz [16]<sup>1</sup>

---

<sup>1</sup>For a critical discussion of this work see Ref. [17].

predicted a one-stage continuous melting transition, i.e. a scenario with a single continuous transition at  $\rho_i = \rho_m$  and consequently without an hexatic phase. Their conclusions were based on the examination of the bond orientational order parameter in very long runs of different systems up to 15876 particles and hard-crystalline wall boundary conditions. Finally, Mitus, Weber and Marx [14] studied the local structure of a system with 4096 hard disks. From the linear behaviour of a local order parameter they derived bounds for a possible coexistence region.

In a recent letter [18] we published the first results of simulations of the hard disk model in the  $NVT$  ensemble with up to 65536 particles to answer the question of the kind of the phase transition. We showed that the behaviour of the susceptibility  $\chi_6$  and the bond orientational correlation length  $\xi_6$  in the isotropic phase as well as the value of the critical exponent  $\eta_6$  coincide with the predictions of the KTHNY theory. Additionally, we performed finite-size scaling (FSS) investigations in the transition region and showed that these results are also in agreement with the KTHNY scenario. Here we discuss the methods in detail and present additional results for the pressure, the topological defect density and the distribution of the second moment of the local bond orientational order parameter. All results are compared with the predictions of the KTHNY theory.

## 2 Algorithm and measurement

As mentioned before, we used MC techniques and the  $NVT$  ensemble for the simulations of the hard disk system. The updating was performed with an improved (non-local) Metropolis algorithm [19]. We consider systems of  $N = 32^2, 64^2, 128^2$  and  $256^2$  hard disks in a two-dimensional square box. We find that finite-size effects with these boundary conditions are not substantially larger than in a rectangular box with ratio  $\sqrt{3} : 2$  since no simulations in the solid phase were made. This point will be discussed later. The simulations were performed on a Silicon Graphics workstation and a CRAY T3E. The CPU time for the CRAY was of the order of some month per node, where we have used 7 or 8 nodes. Further details are described in Ref. [18].

Careful attention has been paid to the equilibration of all systems. We controlled that the expectation values had stabilized over long time. Additionally, we measured some autocorrelation times for smaller systems [19] and estimated the values of larger systems (for large correlations lengths) by assuming  $z \approx 2$ . We spent at least 10% of the time to warm up the system. The measurement frequency was between one measurement per 80 MC ‘sweeps’<sup>2</sup> for  $\rho = 0.82$  and  $N = 64^2$  and one measurement per 5000 MC sweeps for  $\rho = 0.89$  and  $N = 256^2$  since the measurement is expensive compared to the updating steps due to the calculation of neighbours.  $\rho$  is the reduced density since we have set the disk diameter equal to one in the whole paper. The number of measurement sweeps for all performed simulations is collected in Tab. 1. The measured observables will be discussed in the following.

---

<sup>2</sup>A sweep for the chain Metropolis algorithm is defined as  $N$  trials to move chains of particles [19].

Table 1: Number of measurement sweeps that were performed with the chain Metropolis algorithm. The acceptance rate was between 50% and 70%. ‘8 × 1500’ denotes 8 independent data sets with  $1.5 \times 10^6$  sweeps.

$\rho$	sweeps/ $10^3$			
	$N = 32^2$	$N = 64^2$	$N = 128^2$	$N = 256^2$
0.820		$7 \times 1150$		
0.830		$7 \times 1200$		
0.840		$7 \times 1040$		
0.850		$7 \times 1100$		
0.855		$7 \times 840$		
0.860	$8 \times 1500$	$7 \times 960$		
0.865	$8 \times 1500$	$7 \times 640$	$8 \times 430$	
0.870	$8 \times 1600$	$7 \times 620$	$8 \times 470$	
0.875	$8 \times 1700$	$8 \times 500$	$8 \times 430$	
0.880	$8 \times 1500$	$8 \times 600$	$8 \times 450$	1900
0.885	$8 \times 1800$	$8 \times 1200$	$8 \times 520$	1900
0.890	$8 \times 1800$	$8 \times 1100$	$8 \times 550$	$6 \times 1900$
0.895	$8 \times 1800$	$8 \times 800$	$8 \times 630$	
0.897	$8 \times 1800$	$8 \times 1500$	$8 \times 650$	
0.898	$8 \times 1500$	$8 \times 480$	$8 \times 480$	$6 \times 710$
0.900	$8 \times 1500$	$8 \times 640$	$8 \times 370$	
0.905	$8 \times 1500$	$8 \times 590$	$8 \times 410$	
0.910	15000	16500	$8 \times 2200$	

## Bond orientational order parameter and susceptibility

The orientational order of the two-dimensional hard disk system can be described by the (global) bond orientational order parameter  $\psi_6$ . The local value of  $\psi_6$  for a particle  $i$  located at  $\vec{r}_i = (x, y)$  is given by

$$\psi_{6,i} = \frac{1}{N_i} \sum_j \exp(6i\theta_{ij}) , \quad (1)$$

where the sum on  $j$  is over the  $N_i$  neighbours of this particle and  $\theta_{ij}$  is the angle between the particles  $i$  and  $j$  and an arbitrary but fixed reference axis. Neighbours are obtained by the Voronoi construction [20]. The (global) bond orientational order parameter is then defined as

$$\psi_6 = \left| \frac{1}{N} \sum_{i=1}^N \psi_{6,i} \right| . \quad (2)$$

We measured the second and fourth moment of  $\psi_6$ , where the former is related to the susceptibility by<sup>3</sup>

$$\chi_6 = N \langle \psi_6^2 \rangle. \quad (3)$$

## Bond orientational correlation length

The bond orientational correlation function is defined as

$$g_6(\vec{r} - \vec{r}') = \frac{\langle \psi_6^*(\vec{r}) \psi_6(\vec{r}') \rangle}{\langle \rho(\vec{r}) \rho(\vec{r}') \rangle}, \quad (4)$$

where

$$\psi_6(\vec{r}) = \sum_{i=1}^N \delta(\vec{r} - \vec{r}_i) \psi_{6,i} \quad (5)$$

denotes the microscopic bond orientational order-parameter density and

$$\rho(\vec{r}) = \sum_{i=1}^N \delta(\vec{r} - \vec{r}_i) \quad (6)$$

is the microscopic particle density. In the isotropic phase the bond orientational correlation length  $\xi_6$  was extracted from the ‘zero-momentum’ bond orientational correlation function  $g_6(x)$ . This is defined as

$$g_6(x - x') = \frac{1}{L} \iint dy dy' g_6(\vec{r} - \vec{r}'), \quad (7)$$

where  $L$  denotes the box length.

In practice we use the definition

$$g_6(x) \sim \left\langle \left( \frac{1}{N_k} \int_0^L dy \int_{x-\Delta x/2}^{x+\Delta x/2} dx \psi_6(\vec{r}) \right)^* \left( \frac{1}{N'_k} \int_0^L dy' \int_{-\Delta x/2}^{\Delta x/2} dx' \psi_6(\vec{r}') \right) \right\rangle, \quad (8)$$

where

$$N_k = \int_0^L dy \int_{x-\Delta x/2}^{x+\Delta x/2} dx \rho(\vec{r}), \quad (9)$$

$$N'_k = \int_0^L dy \int_{-\Delta x/2}^{\Delta x/2} dx \rho(\vec{r}). \quad (10)$$

Therefore, the distance between two particles in  $x$ -direction is not exactly  $x$ , but lies between  $x - \Delta x$  and  $x + \Delta x$ . Nevertheless, assuming a pure exponential behaviour of the correlation function  $g_6(x)$  the integration over  $\Delta x$  causes no error. In the simulations the value of  $\Delta x$  was given by the length of a cell of the cell structure, i.e.  $\Delta x \approx 2/3$ , where the exact value depends on  $\rho$  and  $N$ .  $g_6(x)$  was fitted with a  $\cosh((L/2 - x)/\bar{\xi}_6)$  in the interval  $x_{\min} \leq x \leq L/2$ , where  $\bar{\xi}_6$  and  $\xi_6$  are related by

$$\frac{1}{2\xi_6} = \sinh\left(\frac{1}{2\bar{\xi}_6}\right). \quad (11)$$

---

<sup>3</sup>This definition yields a factor  $1 - 2/\pi$  in the thermodynamic limit compared to  $\chi_6 = N(\langle \psi_6^2 \rangle - \langle \psi_6 \rangle^2)$ .

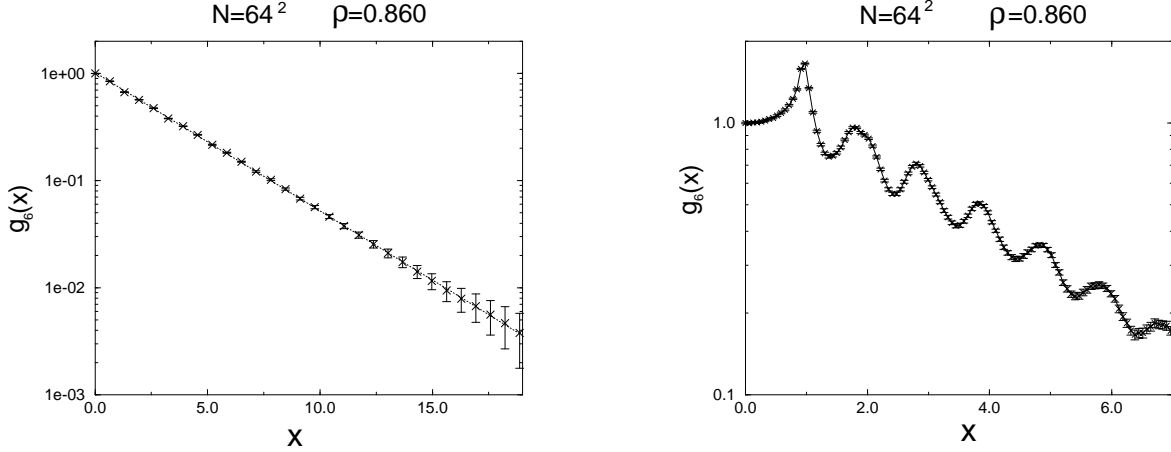


Figure 1: ‘Zero-momentum’ bond orientational correlation function  $g_6(x)$  for  $N = 64^2$  particles at  $\rho = 0.86$  (with arbitrary chosen normalization). The left figure shows the exponential behaviour for large distances, where  $\Delta x$  was about 0.65. The dotted line is the best fit with a hyperbolic cosine ansatz. The right figure illustrates oscillations in  $g_6(x)$  for small distances (with  $\Delta x \approx 0.065$ ). The line is a guide to the eye.

To determine the influence of ‘excitations’ we compare the results for different minimal distances  $x_{\min}$ . The correlations are always dominated by the lowest state of the transfer operator ‘Hamiltonian’, so that it was not necessary to omit points. In Fig. 1 we plot the correlation function for the  $N = 64^2$  particle system at  $\rho = 0.86$  (with arbitrary normalization). The left figure shows the correlation function as obtained from the simulation, i.e. with  $\Delta x \approx 2/3$ . The curve shown is the best fit with a cosh-like behaviour. As one can see there are no influences of ‘excitations’. Although the fit seems to be consistent with the data, there are large deviations. The reason is an oscillating behaviour of  $g_6(x)$  as shown in the right figure, where we have chosen  $\Delta x$  ten times smaller. The same oscillations can be seen, if we plot the relative deviations between the data of the first case ( $\Delta x \approx 2/3$ ) and the hyperbolic cosine fit. This is done in Fig. 2. Since the oscillating length is about 1, the curve can be smoothed if one chooses  $\Delta x \approx 1$ . Nevertheless, also with  $\Delta x \approx 2/3$  a precise determination of the correlation length is possible. Systematic errors coming from the oscillations are taken into account. These errors get dominant — compared to our statistical errors — for small values of  $\xi_6$ .

## Radial bond orientational correlation function

In the isotropic phase  $g_6(\vec{r})$  is independent of the angle. Therefore, we use the angle averaged quantity

$$g_6(r) \sim \langle \psi_6^*(0) \psi_6(r) \rangle / g(r) \quad (12)$$

for an additional calculation of  $\xi_6$ , where  $g(r)$  is the (radial) pair correlation function. The radial bond orientational correlation function  $g_6(r)$  was fitted for large distances with an

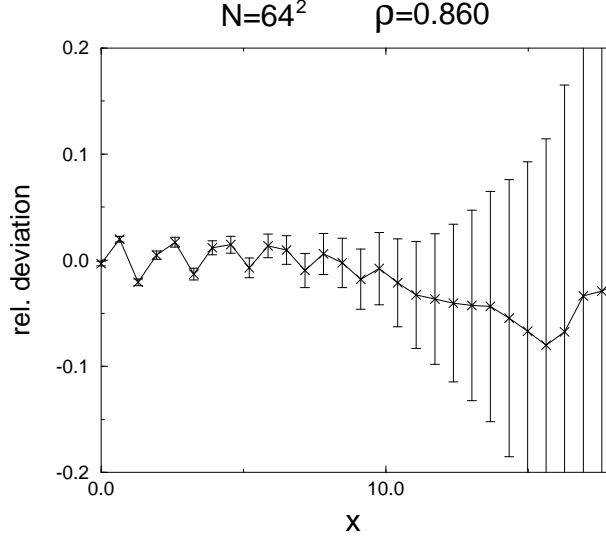


Figure 2: Relative deviations of  $g_6(x)$  (left picture in Fig. 1) from a hyperbolic cosine fit.

ansatz of the form

$$g_6(r) \sim r^{-\eta_6} \exp(-r/\xi_6) . \quad (13)$$

In Fig. 3 we plot  $g_6(r)$  for  $N = 64^2$  hard disks at  $\rho = 0.86$ . The left figure shows the oscillating behaviour of  $g_6(r)$ . In order to smooth the curves,  $g_6(r)$  has been averaged over a distance of one. This was done in the right figure, where  $g_6(r)$  was additionally multiplied by  $r^{\eta_6}$  in order to compare the data with an exponential behaviour.

The values of  $\xi_6$  obtained from  $g_6(r)$  are affected by larger systematic errors (compared to the previous method). The reason is that one has to leave out the points with very small and very large distances. The first points have to be omitted since the ansatz is not valid in this case, while points with  $r \approx L$  are affected by finite-size effects. In contrast to  $g_6(x)$ , where the periodicity just leads to a cosh behaviour,  $g_6(r)$  has no simple periodic behaviour. Therefore, one has to omit the points with large  $r$ . Nevertheless, we use the radial bond orientational correlation function for a determination of the correlation length. In all cases both values of  $\xi_6$  coincide within the statistical errors.

## Pressure

The pressure was calculated from the pair correlation function  $g(r)$  in the range  $1.0 < r < 1.2$ . From 200 bins we extracted the contact value of the pair correlation function by fitting the data with a power series of sixth order and extrapolating to  $g(1)$ . The virial theorem relates this value to the pressure by [21]

$$\frac{pA_0}{NkT} = \frac{\sqrt{3}}{2} \rho \left( 1 + \frac{\pi}{2} \rho g(1) \right) , \quad (14)$$

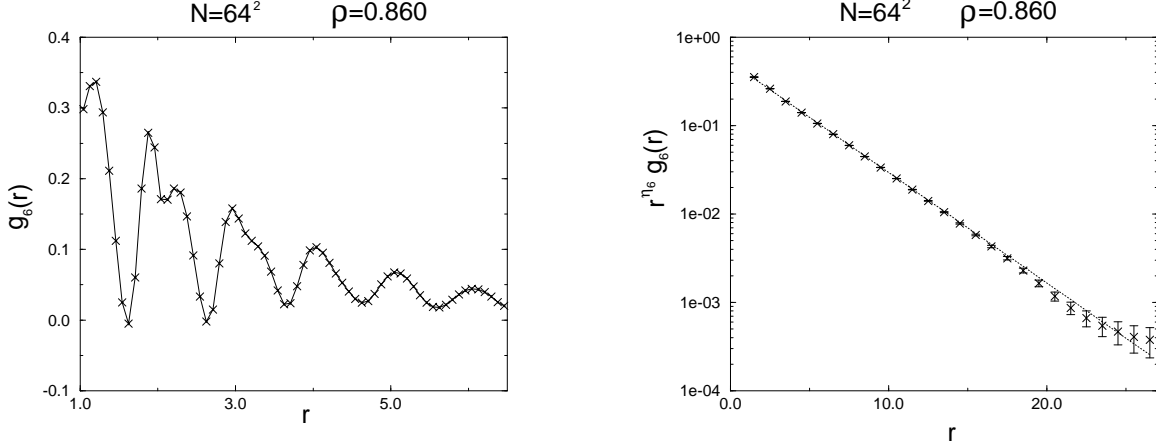


Figure 3: Radial bond orientational correlation function  $g_6(r)$ . The left figure shows the behaviour for small distances. The line is just a guide to the eye. In the right figure we plot  $r^{\eta_6} g_6(r)$  together with an exponential fit (dotted line).

where  $A_0$  is the closed-packed area of the system, i.e.  $A_0 = N\sqrt{3}/2$ . Statistical errors were calculated by independent data sets and by performing fits on the whole data sets to a Gaussian distribution of  $g(r)$  with variance  $\Delta g(r)$ . Systematic errors were estimated by changing the order of the power series from six to five.

Our results for the pressure as a function of the system size and the density are collected in Tab. 2 and visualized in Fig. 4. The quoted error is the sum of the statistical and systematic error. The data show the end of the liquid region and the beginning of a possible liquid-solid tie line, while no simulations in the solid phase were made. For densities up to  $\rho = 0.885$ , the pressure does not have any finite-size effect within the statistical errors. Taking the finite-size dependency of the pressure together with the data of  $\xi_6$  (which are discussed in Sec. III), we find that we have reached the thermodynamic limit for the systems with  $N = 128^2$  particles up to  $\rho = 0.885$  and for the systems with  $N = 256^2$  particles up to  $\rho = 0.89$ . For densities  $\rho > 0.89$  there might be still finite-size effects. The results are consistent with those of Zollweg and Chester [12], who used the same methods but a rectangular box with ratio  $\sqrt{3} : 2$ . Only the value at  $\rho = 0.910$  shows deviations. This could be a result of the square box, which leads to larger finite size effects if the density of the system is near the solid phase. Another possibility is that the large systems at higher densities are not fully equilibrated. However, this seems to be unlikely due to our observation of the pressure as a function of time. Our results give a lower bound for the beginning of a coexisting phase of  $\rho \approx 0.89$ , but give neither any conclusive evidence for a first-order phase transition or an hexatic phase. It just shows that the compressibility in this region is very high.

## Local bond orientational order parameter

The distribution of the second moment of the local bond orientational order parameter  $|\psi_{6,i}|^2$  was first studied by Strandburg, Zollweg and Chester [22]. In the case of a first-order



Table 2: Pressure for densities in or near the transition region.

$\rho$	$pA_0/NkT$			
	$N = 32^2$	$N = 64^2$	$N = 128^2$	$N = 256^2$
0.880	7.803(5)	7.799(6)	7.796(7)	7.795(8)
0.885	7.894(5)	7.900(6)	7.899(8)	7.895(9)
0.890	7.926(5)	7.950(7)	7.950(9)	7.953(5)
0.895	7.910(6)	7.953(9)	7.963(9)	
0.897	7.905(6)	7.940(6)	7.956(7)	
0.898	7.892(6)	7.934(9)	7.955(5)	7.954(4)
0.900	7.897(7)	7.928(9)	7.951(7)	
0.905	7.906(6)	7.901(9)	7.943(8)	
0.910	7.916(5)	7.900(5)	7.928(5)	

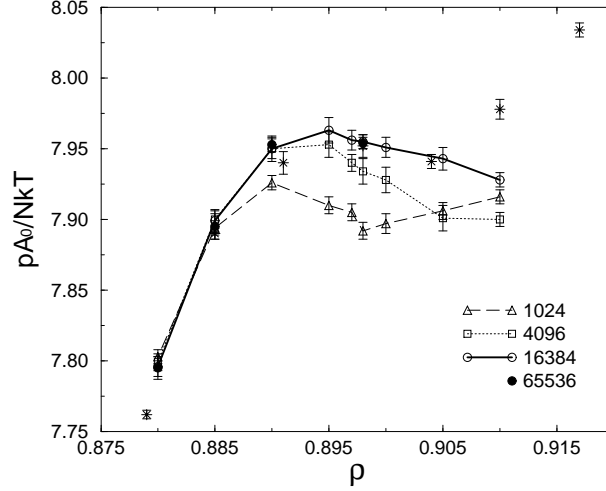


Figure 4: Pressure as a function of the density for various system sizes. Data of Ref. [12] are marked by stars.

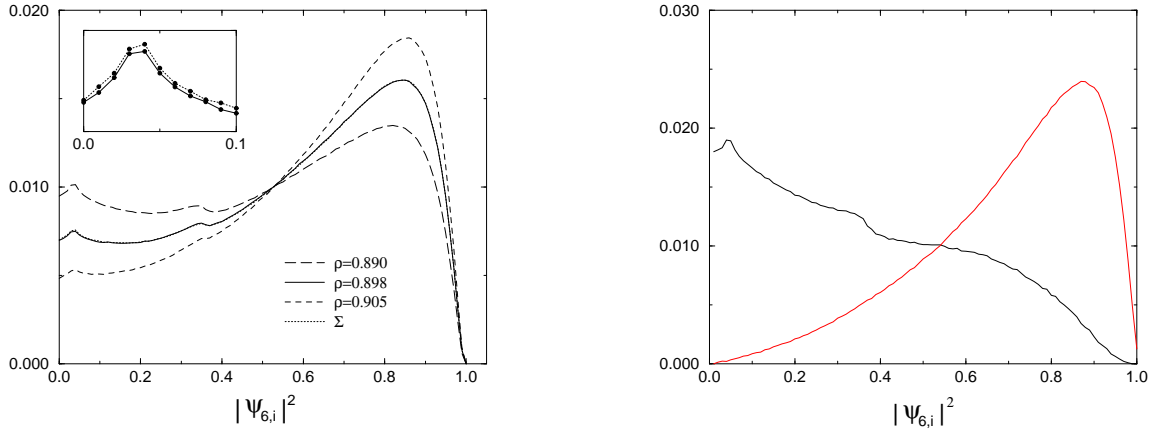


Figure 5: The left figure shows the distribution occurrence of the second moment of the local bond orientational order parameter  $|\psi_{6,i}|^2$  (in arbitrary units) for  $N = 128^2$  hard disks at three different densities.  $\Sigma$  indicates the curve, which is the linear combination of  $\rho_1 = 0.89$  and  $\rho_2 = 0.905$ . The small inset amplifies the region with small  $|\psi_{6,i}|^2$  to show the small difference between the direct measurement and the linear combination. Errors are of the order of the distance between the two curves. The right figure displays two distributions, which can be taken as the initial distributions for the modelling of all others in the transition region.

phase transition (with thin interfaces) one expects that the distribution of the coexistence phase is the sum of the fluid, solid and interface distribution weighted with their relative areas. On the left picture of Fig. 5 we plot  $|\psi_{6,i}|^2$  for systems with 16384 hard disks at three different  $\rho$ 's. To check if the distribution at  $\rho = 0.898$  corresponds to a coexisting phase, we compare it with a combination of two other distributions at  $\rho_1$  and  $\rho_2$ , respectively. It is not necessary that the two chosen densities ( $\rho_1$  and  $\rho_2$ ) are the exact values of lowest and highest density of a possible coexisting region. This should work for two arbitrary densities, provided that these systems are in the coexisting phase. If a first-order phase transitions exists, but the chosen density of  $\rho_1 = 0.89$  is too low or  $\rho_2 = 0.905$  is too high, there are deviations. Obviously, the direct measurement and the modelling are in perfect agreement. Moreover, the weights of the two distributions correspond to their theoretical values of  $8/15$  and  $7/15$ , respectively. Nevertheless, an interpretation as the sum of two distributions from two different phases of a first-order phase transition makes only sense if the system size is larger than the two interfaces. But the results of the following sections will show that a first-order phase transition with such small interfaces can be ruled out. Therefore the situation is more complicate than in this simple picture.

The distributions of  $|\psi_{6,i}|^2$  in the transition region can be modelled as the sum of two initial distributions. The reconstruction of these distributions is not unique. A decomposition is shown in the right picture of Fig. 5. One of the distributions results primary from particles with six neighbours, while the other is mainly the sum of distributions from

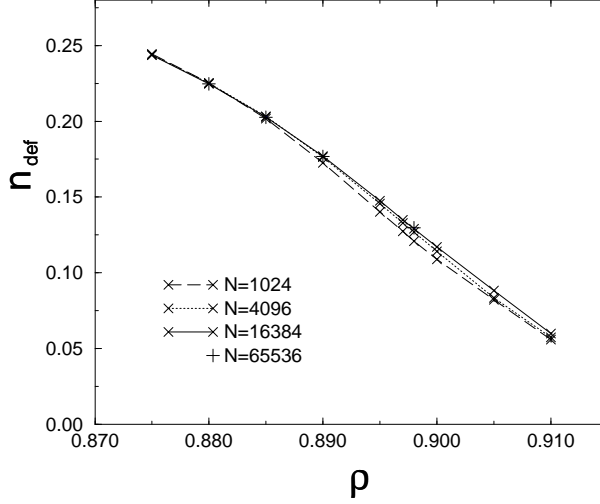


Figure 6: Topological defect density  $n_{\text{def}}$  as a function of  $\rho$ . Statistical errors are too small for a visualization.

particles with coordination numbers unequal six.

Additional investigations for the dependency of the distribution of  $|\psi_{6,i}|^2$  on the system size are discussed in Sec. IV.

## Topological defects

An analysis of the numbers of neighbours of each particle as obtained from the Voronoi construction gives a characterization of the defect structure of a two-dimensional system. The average number of neighbours is — independent of the state of disorder — six. In a perfect solid each particle has six neighbours. Particles with any other number of neighbours represent a disclination. Dislocations are pairs of disclinations. We define the density of defects as

$$n_{\text{def}} = \frac{1}{N} \sum_{i \neq 6} N_i^{\text{Nb}}, \quad (15)$$

where  $N_i^{\text{Nb}}$  denotes the number of particles with  $i$  neighbours. Alternatively one can take the strengths of the disclinations into account and define the density of defects as

$$n'_{\text{def}} = \frac{1}{N} \sum_i |i - 6| N_i^{\text{Nb}} = \frac{2}{N} \sum_{i < 6} (6 - i) N_i^{\text{Nb}}. \quad (16)$$

However, the difference between the two definitions for  $\rho \geq 0.88$  is lower 1%.

In Fig. 6 we plot  $n_{\text{def}}$  as a function of  $\rho$ . One can see that there is a linear behaviour of  $n_{\text{def}}$  for  $\rho \geq 0.89$ <sup>4</sup>. As in the case of the distribution of  $|\psi_{6,i}|^2$ , this could be explained with the coexistence of two different phases. However, if one examines the defect structure of

<sup>4</sup>A linear behaviour of a local order parameter was also found in Ref. [14].

several configurations in the transition region and the configurations itself, one finds no hint for two coexisting phases, while they are compatible with the picture of a homogeneous phase. Therefore, the conventional picture (of a first-order phase transition with thin interfaces) of two separated phases is incompatible with the data. The results of Sec. IV will confirm this assumption.

There are different possibilities to explain this linear behaviour. On the one hand there could be a weak first-order phase transition with an interface width which is larger than the box length  $L$  of our largest system of  $N = 256^2$  particles, on the other hand a continuous transition with a homogeneous phase. In both cases increasing the density  $\rho$  primary leads to a decrease of the defect density, since the average density in the ordered regions is higher than the density in unordered regions (i.e. a disclination or dislocation needs more space than perfect crystalline structures). In the case of a first-order phase transition the defects will form some larger structure, while there is a homogenous distribution for the continuous transition.

### 3 Simulation in the isotropic phase

In the isotropic phase we measured the susceptibility and the correlation length of the bond orientation. Subsequently, we compare the results with the predictions of the KTHNY theory, i.e. a critical exponent  $\eta_6$  of  $1/4$  and an exponential singularity for the correlation length

$$\xi_6(t) = a_\xi \exp(b_\xi t^{-1/2}) \quad (17)$$

and the susceptibility

$$\chi_6(t) = a_\chi \exp(b_\chi t^{-1/2}) \quad (18)$$

if  $t = \rho_i - \rho \rightarrow 0^+$ . A detailed description of these measurements is given in Ref. [19].

Our results of  $\chi_6$  and  $\xi_6$  as a function of the density are summarized in Tab. 3. We analyzed the critical behaviour of  $\chi_6(\rho)$  and  $\xi_6(\rho)$  by performing least square fits according to Eqs. (17) and (18). Using all 12 points we got a  $\chi^2$  per degree of freedom (d.o.f.) of 0.75 for  $\xi_6(t)$  and 0.65 for  $\chi_6(t)$ , i.e. the data are in a very good agreement with an exponential singularity of the KTHNY type. This is not only a result of large statistical errors as can be seen if one uses different approaches for the singularities. For example, a conventional second-order behaviour with a power-law singularity of the form  $\ln(\xi_6) = a - \nu \ln(t)$  yields  $\chi^2/\text{d.o.f.} = 4.1$ .

All results for the fit parameter are collected in Tab. 4. The values for  $\chi_6(\rho)$  and  $\xi_6(\rho)$  together with the fitted curves are shown in Fig. 7. We also made fits where we have omitted some data at lower densities. The fit parameters for  $\chi_6(\rho)$  show only non-essential changes, while the changes for  $\xi_6(\rho)$  are of the order of the statistical errors. An analysis of the behaviour of  $\ln(\chi_6/\xi_6^{7/4})$  as a function of  $\ln(\xi_6)$  yields the following value of the critical exponent:

$$\eta_6 = 0.251(36) . \quad (19)$$

Table 3: Bond orientational correlation length  $\xi_6$  and susceptibility  $\chi_6$  for various densities in the isotropic phase.  $N$  refers to the system sizes used.

$\rho$	$N$	$\xi_6$	$\chi_6$
0.82	$64^2$	1.513(50)	3.797(13)
0.83	$64^2$	1.800(35)	4.693(15)
0.84	$64^2$	2.156(40)	6.052(24)
0.85	$64^2$	2.635(30)	8.415(41)
0.855	$64^2$	2.995(35)	10.30(6)
0.86	$64^2$	3.425(40)	12.96(9)
0.865	$64^2, 128^2$	4.14(10)	17.45(18)
0.87	$128^2$	5.03(15)	25.00(39)
0.875	$128^2$	6.65(30)	39.5(8)
0.88	$128^2, 256^2$	9.56(26)	75.0(21)
0.885	$128^2, 256^2$	15.65(51)	176.8(61)
0.89	$256^2$	38.0(15)	865(44)

## 4 Simulation in the transition region

We now come to the simulations with  $\rho \approx \rho_i$ . Finite-size scaling (FSS) implies for the susceptibility

$$\chi_6 \sim L^{2-\eta_6} f(L/\xi_6) . \quad (20)$$

Assuming the prediction of the KTHNY theory, the correlation length  $\xi_6$  diverges at  $\rho = \rho_i$  and  $f$  is a constant independent of  $L$ . We use this FSS behaviour to locate  $\rho_i$ , where we take  $\eta_6 = 1/4$ . In the hexatic phase ( $\rho_i < \rho \leq \rho_m$ ) the correlation length  $\xi_6$  also diverges, so that  $f$  is still independent of  $L$ . In this phase  $\eta_6$  is a decreasing function of the density which goes to zero if  $\rho$  approaches the melting density  $\rho_m$ , i.e. at the end of the hexatic phase. For  $\rho$ 's below  $\rho_i$ , one has to take corrections of  $\chi_6 \sim L^{2-\eta_6}$  for finite correlations lengths into account. Our results for the susceptibility are collected in Tab. 5.

Table 4: Best fit parameter for the critical behaviour of the correlation length and susceptibility. For  $0.82 \leq \rho \leq 0.89$  we have fitted 12 points, while we used 8 points in the range  $0.855 \leq \rho \leq 0.89$ .

Fit	range	$\ln(a)$	$b$	$\rho_i$	$\chi^2/\text{d.o.f.}$
$\xi_6(\rho)$	$0.82 \leq \rho \leq 0.89$	-1.44(8)	0.547(21)	0.9017(6)	0.75
$\xi_6(\rho)$	$0.855 \leq \rho \leq 0.89$	-1.27(13)	0.505(31)	0.9006(8)	0.23
$\chi_6(\rho)$	$0.82 \leq \rho \leq 0.89$	-1.65(3)	0.847(7)	0.9002(3)	0.65
$\chi_6(\rho)$	$0.855 \leq \rho \leq 0.89$	-1.60(9)	0.834(21)	0.9000(4)	0.58

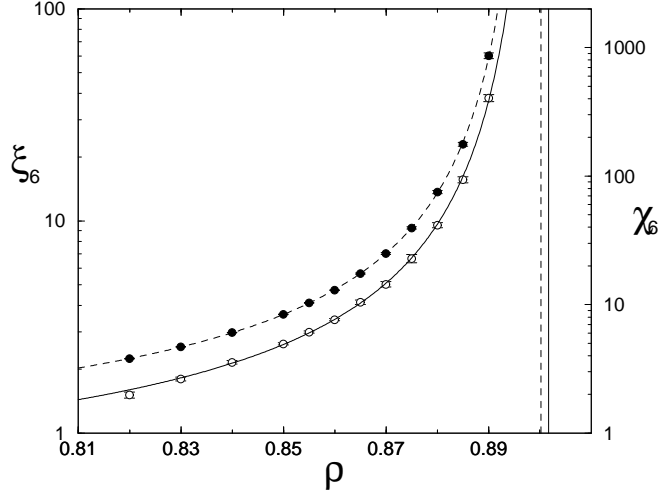


Figure 7: Susceptibility (full symbols) and bond orientational correlation length (open symbols) as a function of density. The curves shown are the best fits for a KTHNY behaviour (for all measured points). The critical values of  $\rho$  are visualized by vertical lines.

If we use the FSS behaviour to locate  $\rho_i$  and  $\rho_m$ , then the requirement of  $\eta_6(\rho_i) = 1/4$  yields [19]

$$\rho_i = 0.899(1) , \quad (21)$$

while  $\eta_6(\rho_m) = 0$  leads to the estimate  $\rho_m \gtrsim 0.91$ . The value of  $\rho_i$  is in agreement with that obtained from the singularities of  $\xi_6(t)$  and  $\chi_6(t)$ . A slightly different value of  $\eta_6$  (from the relation of  $\chi_6$  and  $\xi_6$  in the isotropic phase) would not change this situation. Moreover, our values of  $\rho_i$  are in agreement with the result of Weber et al. [13] obtained from the fourth-order cumulant intersection ( $\rho_i = 0.8985(5)$ ). However, it differs from their value obtained using the singularity of  $\chi_6$  ( $\rho_i = 0.913$ ). The result  $\rho_i = 0.916(4)$  of Fernández et al. [16] is not compatible with our value.

Another quantity which can be used to analyze the kind of the transition is the fourth-order cumulant

$$U = 1 - \frac{\langle \psi_6^4 \rangle}{3 \langle \psi_6^2 \rangle^2} . \quad (22)$$

According to the prediction of the KTHNY theory,  $U$  should be independent of the system size  $L$  in the whole hexatic phase. In contrast to this, in the case of a conventional first-order phase transition there is only a single point, where the cumulants of different system sizes collapse. Since there is a large region between  $\rho_i \approx 0.9$  and  $\rho_m \gtrsim 0.91$ , the behaviour of  $U$  can be used to distinguish between a KTHNY and a first-order transition. The intersection of the cumulant  $U$  in a single point was an argument in Ref. [13] against the existence of an hexatic phase. Unfortunately, statistical errors in our data are too large to answer this question as can be seen in Fig. 8.

Table 5: The susceptibility per particle in the transition region.

$\rho$	$\chi_6/N$			
	$N = 32^2$	$N = 64^2$	$N = 128^2$	$N = 256^2$
0.895	0.2620(9)	0.1970(17)	0.1409(24)	
0.897	0.2987(9)	0.2418(18)	0.1899(25)	
0.898	0.3175(10)	0.2612(17)	0.2160(25)	0.1788(29)
0.900	0.3514(10)	0.3076(13)	0.2630(17)	
0.905	0.4235(19)	0.4055(11)	0.3745(13)	
0.910	0.4900(29)	0.4840(24)	0.4707(10)	

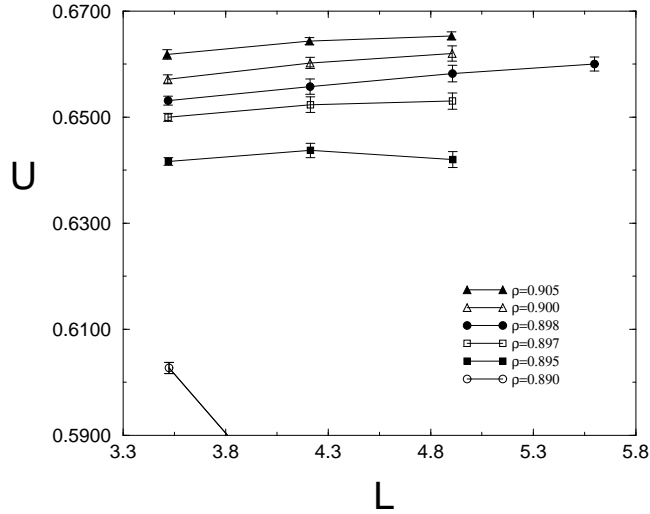


Figure 8: Finite-size scaling of the cumulant in the transition region.

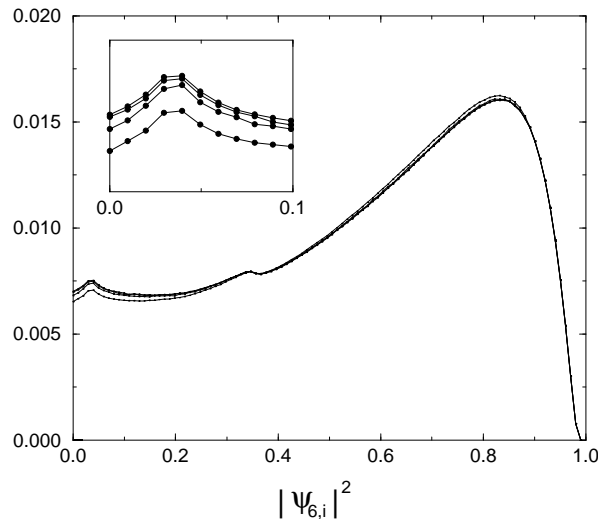


Figure 9: Distribution of the second moment of the local bond orientational order parameter (in arbitrary units) for different system sizes. The small inset amplifies the region with small  $|\psi_{6,i}|^2$ , where are the largest deviations. Statistical errors are of the order of the symbols in the inset.

Another possibility to distinguish a first-order phase transition from a continuous transition is to study the dependency of the distribution of  $|\psi_{6,i}|^2$  on the size of the system. If the system exhibits a homogeneous hexatic phase, then changing the size of the system should not lead to any changes in the distribution. On the other hand, if the transition is of first order one would expect that the distribution is a combination of the solid, fluid and interface distribution. Therefore, changing the size of the system would result in a change of the distribution, because the area of the interface scales only linear with  $L$ . In Fig. 9 we plot  $|\psi_{6,i}|^2$  at  $\rho = 0.898$  for four different system sizes. Apart from finite-size effects, which getting weaker for larger systems, no difference between the distributions can be seen. The distributions for the two largest systems coincide within statistical errors. Therefore, one can rule out a first-order transition with thin interfaces<sup>5</sup>, while a first-order transition with an interface width larger than the largest system size  $L$  and a continuous transition are compatible with the data. These results coincide with those of Fernández et al. [16], who performed similar measurements in the  $NpT$  ensemble using a rectangular box of ratio  $\sqrt{3} : 2$ . The data of Fig. 9 show also that the chosen ratio of the side lengths of 1 : 1 causes no large finite-size effects.

---

<sup>5</sup>The results are also compatible with the occurrence of two very small interfaces (i.e. a width of  $\mathcal{O}(1)$ ), but this can be ruled out due to the examination of the defect structure of several configurations.



## 5 Conclusions and outlook

We presented a detailed Monte Carlo study of the two-dimensional hard disk model in the  $NVT$  ensemble. The investigations were performed in the isotropic phase and in the transition region.

The behaviour of the defect density as well as the distribution of the local order parameter in the transition region were in good agreement with a simple model of two coexisting phases, i.e. the data could be modelled as the sum of two different phases, where the relative areas of the two phases are proportional to  $\rho$ . However, the defect structure of the system and the distribution of  $|\psi_{6,i}|^2$  as a function of  $L$  showed, that there are not two separated phases with a thin interface. The data can be explained by a weak first-order transition with a width of the interface which is larger than the largest system size  $L$  or by a continuous transition with a homogeneous phase.

The behaviour of the pressure was compatible with both a first-order and a KTHNY-like scenario. The data just give a lower limit of  $\rho \approx 0.89$  for the coexisting phase.

In the isotropic phase we examined the dependency of the correlation length and the susceptibility on the density  $\rho$ . We showed that the data are in good agreement with the prediction of an exponential singularity from the KTHNY theory. The critical exponent  $\eta_6$  was derived from the relation on  $\xi_6$  and  $\chi_6$  for  $\xi_6 \rightarrow \infty$ . We got  $\eta_6 = 0.251(36)$ , which coincides with the prediction  $\eta_6 = 1/4$ .

The simulations in the transition region were used to measure the finite-size scaling of the susceptibility. The value of  $\rho_i = 0.899(1)$  (assuming  $\eta_6 = 1/4$ ) coincided with those from the KTHNY-like behaviour of  $\xi_6(\rho)$  and  $\chi_6(\rho)$ . Furthermore, the requirement  $\eta_6(\rho_m) = 0$  led to the estimate  $\rho_m \gtrsim 0.91$ . The data of the fourth-order cumulant  $U$  were affected by too large statistical errors in order to draw any conclusions.

In summary, all data are compatible with a KTHNY-like phase transition. A one-stage continuous transition ( $\rho_i = \rho_m$ ) as proposed in Ref. [16] and a first-order transition with small correlation length can be ruled out<sup>6</sup>. Further numerical investigations have to be performed to make a clear decision between a weak first-order phase transition and a continuous scenario. This could be done for example by studying the positional order in the transition region. Work along this line is in progress.

## Acknowledgments

We thank Harro Hahn for helpful discussions and the Institute of Scientific Computing in Braunschweig for providing computer time on their CRAY T3E. Especially we benefit from discussions with Rainer Gensch.

## References

- [1] K.J. Strandburg, Rev. Mod. Phys. **60** (1988) 161.
- [2] M.A. Glaser, N.A. Clark, Adv. Chem. Phys. **83** (1993) 543.

---

<sup>6</sup>Similar results are obtained for an  $r^{-12}$  repulsive potential by Bagchi, Andersen and Swope [23].

- [3] N.D. Mermin, H. Wagner, Phys. Rev. Lett. **17** (1966) 1133.
- [4] J.M. Kosterlitz, D.J. Thouless, J. Phys. C **6** (1973) 1181; J.M. Kosterlitz, J. Phys. C **7** (1974) 1046; B.I. Halperin, D.R. Nelson, Phys. Rev. Lett. **41** (1978) 121; A.P. Young, Phys. Rev. B **19** (1979) 1855.
- [5] S.T. Chui, Phys. Rev. Lett. **48** (1982) 933; Phys. Rev. B **28** (1983) 178.
- [6] V.N. Ryzhov, E.E. Tareyeva, Phys. Rev. B **51** (1995) 8789.
- [7] Y. Saito, Phys. Rev. Lett. **48** (1982) 1114; Phys. Rev. B **26** (1982) 6239.
- [8] W. Janke, H. Kleinert, Phys. Rev. Lett. **61** (1988) 2344 and references therein.
- [9] A. Jaster, H. Hahn, Physica A **252** (1998) 199.
- [10] B.J. Alder, T.E. Wainwright, Phys. Rev. **127** (1962) 359.
- [11] J.A. Zollweg, G.V. Chester, P.W. Leung, Phys. Rev. B **39** (1989) 9518.
- [12] J.A. Zollweg, G.V. Chester, Phys. Rev. B **46** (1992) 11186.
- [13] H. Weber, D. Marx, K. Binder, Phys. Rev. B **51** (1995) 14636; H. Weber, D. Marx, Europhys. Lett. **27** (1994) 593.
- [14] A.C. Mitus, H. Weber, D. Marx, Phys. Rev. E **55** (1997) 6855.
- [15] J. Lee, K.J. Strandburg, Phys. Rev. B **46** (1992) 11190.
- [16] J.F. Fernández, J.J. Alonso, J. Stankiewicz, Phys. Rev. Lett. **75** (1995) 3477; Phys. Rev. E **55** (1997) 750.
- [17] H. Weber, D. Marx, Phys. Rev. Lett. **78** (1997) 398; J.F. Fernández, J.J. Alonso, J. Stankiewicz, Phys. Rev. Lett. **78** (1997) 399.
- [18] A. Jaster, Europhys. Lett. **42** (1998) 277.
- [19] A. Jaster, preprint cond-mat/9711256 (to be published in Physica A).
- [20] For a definition of Voronoi cell see: D.P. Fraser, M.J. Zuckerman, O.G. Mouritzen, Phys. Rev. A **42** (1990) 3186.
- [21] N. Metropolis, A.W. Rosenbluth, M.N. Rosenbluth, A.H. Teller, E. Teller, J. Chem. Phys. **21** (1953) 1087.
- [22] K.J. Strandburg, J.A. Zollweg, G.V. Chester, Phys. Rev. B **30** (1984) 2755.
- [23] K. Bagchi, H.C. Andersen, W. Swope, Phys. Rev. Lett. **76** (1996) 255; Phys. Rev. E **53** (1996) 3794.